Int J Adv Manuf Technol (2016) 82:1675–1682
DOI 10.1007/s00170-015-7446-y

ORIGINAL ARTICLE

Phase and stress evolution in diamond microparticles during diamond-coated wire sawing of Si ingots

Junting Yang[1] · Sriya Banerjee[1] · Junnan Wu[1] · Yoon Myung[1] · Omid Rezvanian[2] · Parag Banerjee[1]

Received: 19 March 2015 / Accepted: 15 June 2015 / Published online: 10 July 2015

Abstract Diamond microparticles undergo changes to their structure and stress state during diamond-coated wire sawing of Si ingots. This phenomenon is revealed using confocal, micro-Raman spectroscopy of diamond microparticles attached to wires which perform the sawing action. Post-wafer-sawed diamonds show the appearance of D (1350 cm^{-1}) and G (1597 cm^{-1}) bands of graphite besides the characteristic diamond T_{2g} band at 1332 cm^{-1}. The graphitic phase extends inside the diamond to a depth of ~14 μm. The ratio of the intensities of D and G bands allows an estimate of the graphitic crystallite size. The grain size varies from 10 nm close to the surface to 53 nm near the graphite/diamond interface. On other diamonds, blue shifts in the T_{2g} peak position are observed indicating the presence of compressive stress. The peak shifts (up to 3.6 cm^{-1}) are anisotropic, i.e., along the direction of wire cutting, and are estimated to be 2.9 GPa. It is proposed that the cumulative effect of compressive stresses over multiple cutting events during the sawing process can lead to local graphitization of diamond particles, thus contributing to loss in cutting efficiency.

Keywords Diamond · Graphitization · Diamond-coated wire sawing · Raman spectroscopy

✉ Parag Banerjee
parag.banerjee@wustl.edu

[1] Department of Mechanical Engineering & Materials Science, Washington University in St. Louis, One Brookings Drive, St. Louis, MO 63130, USA

[2] SunEdison, 501 Pearl Drive, St Peters, MO 63376, USA

1 Introduction

Diamond-coated wire (DCW) sawing process is a highly efficient technique for rapid wafering of solar-grade Si ingots [1]. Diamond particles of ~20-μm size are attached via electrochemical Ni deposition to the surface of a stainless steel wire ~100 μm in diameter. These fixed diamond particles perform the cutting action while traversing inside cut grooves at velocities of ~15 m/s (Fig. 1a, b). The main advantages of this technique are that higher rates of cutting are achieved, fewer consumables are used with minimal environmental impact (since the use of slurry and abrasive particles is obviated), and Si kerf losses are minimized.

In order to understand the cutting process of DCWs, the interaction of diamond with Si needs to be understood. Initial understanding of the mechanical interaction between diamond and Si was based upon scratch studies using diamond scribes on Si [2, 3]. The presence of a metastable, metallic Si phase was established during the diamond scribing process. This metallic phase raised the attractive possibility of ductile machining of Si under high stress conditions.

Studies with diamond indenters [4] and tools [5–8] working on Si wafer surfaces have revealed both brittle and ductile modes of machining. It was found that ductile chipping occurred when diamond tool tip radii were less than ~800 nm [7, 6]. For larger tool radius, brittle fracture occurred as larger chunks fractured from the Si surface and became the primary mode of material removal. The effect of additional tool and machining parameters such as diamond tool shape, crystalline orientation, temperature, and pressure on the cutting of Si was illustrated as well [5, 9, 10].

While these results are important to gain practical knowledge of diamond machining of Si in general, the process of DCW sawing is far more complicated. The diamond particle density, size and size distribution, shape, and orientation all

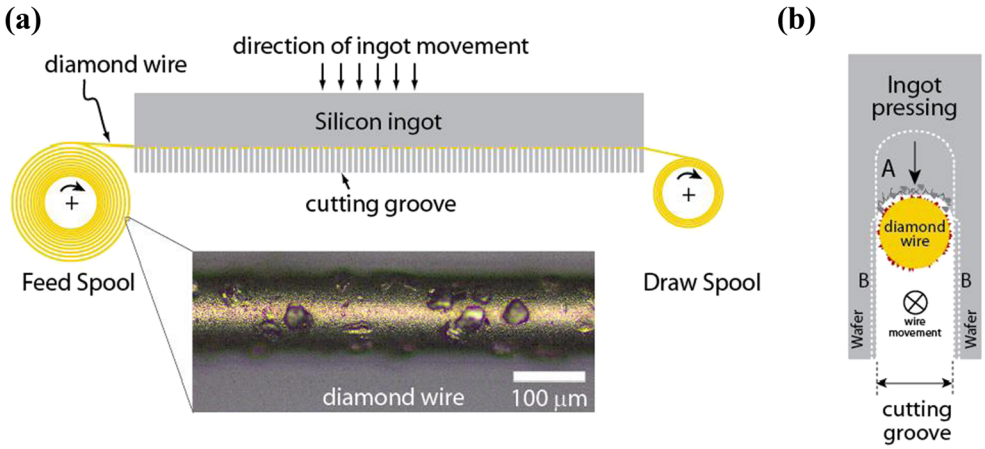

Fig. 1 **a** DCW sawing setup shows a spool of DCW interlaced through the cutting grooves. The silicon ingot moves down as the DCW moves at velocities ~15 m/s in and out of the plane of the figure. An optical micrograph of the DCW is also shown. **b** Cross section of the cutting groove between two would-be wafers shows the cutting action in regions defined as *A*, where rapid and brittle fracture is required, and *B*, where more ductile mode of machining is required for a smoother surface finish of the final wafer. The single DCW is moving inside the plane of the paper (defined by *encircled x* symbol)

play a critical role in determining the efficiency (i.e., the rate) of the cutting process. The stochastic nature of the process can be appreciated by recognizing that every diamond particle spends some time (1) removing material along the cut direction within the ingot slot (region marked "A" in Fig. 1b), (2) scratching the surface of the would-be wafer (region marked "B" in Fig. 1b) or (3) not participating in the cutting process at all. Rapid and successive cutting events at high strain rates make the process difficult to analyze quantitatively.

Depending on the state of the diamond, brittle fractures may result in removal of Si particle or ductile shavings may be produced. Brittle fractures are preferable for faster cutting, while ductile removal of material will provide smoother Si wafer surfaces. Further, diamonds may (1) dislodge themselves under large shear forces, (2) lose their cutting ability due to blunting action of the Si, or (3) undergo graphitization under extreme stress conditions. In all of the above cases, loss in efficiency of the cutting process is expected.

Studies of the DCW cutting of Si ingots have been made [11–13]. These reports have focused on the Si wafer but do not shed light on the cutting mechanism of the DCW. Mapping the chemical and physical characteristics of the interaction of the DCW with Si will help to formulate a detailed understanding of the fundamental processes that drive DCW-based Si cutting.

In this paper, we investigate the effects of Si cutting on the diamond particles embedded on a cutting wire. This is done using Raman spectroscopy of individual diamond particles. Raman spectroscopy is a technique to monitor bond vibrations in a material [14]. The method is non-destructive and does not require sample preparation or a vacuum chamber for analysis. Further, with acquisition times in the range of 5–10 s, the measurement is relatively quick. Together with a microscope stage with XYZ motion control, depth profiling (i.e., confocal) and area mapping of materials can easily be conducted.

Si and the allotropes of carbon–diamond (sp^3-bonded) and graphite (sp^2-bonded) are the classic examples of materials studied using Raman spectroscopy. However, the impact on diamond particles during Si wafering has not been studied till date. Raman spectroscopy is uniquely suited to study diamond machining due to the exceptionally large Raman cross section (i.e., sensitivity) of the C–C bond in its graphitic (sp^2) form. Any changes to the bonding environment ($sp^3 \rightarrow sp^2$) can easily be detected by Raman.

We report on observing a graphitic phase on the cutting face of a diamond particle used for Si wafering. Regardless of the source, a graphitic phase on the cutting face of a diamond particle can lead to a loss in cutting efficiency, even though the diamond remains affixed to the stainless steel wire. Further, we show that in cases where the particles maintain their diamond crystal structure, Raman peak shifts are observed that are consistent with highly directional stresses experienced when diamonds are compressed against Si during cutting. Thus, diamond particles subjected to Si cutting undergo changes in their stress state and under extreme conditions may transform to the softer, graphitic phase.

2 Experimental

Fresh and used DCWs were obtained from SunEdison, Inc. The cutting wires were made of stainless steel 100 μm in diameter, with microsize diamonds at high density (120–140 pieces per 1.2-mm length of wire) covering the surface. Diamond particles were embedded using a Ni electroplating process [15]. Diamond particles on a fresh wire were initially coated under the Ni film and then exposed during the cutting process. The cutting process

was carried at a wire speed of 15 m/s. The table speed (i.e., speed at which the ingot was pressed against the wires) of the ingot was maintained at 1 mm/min. The Si ingot measured 15.6×15.6×100 cm (W×H×L).

The diamond-coated wires are tens of kilometers long, rolled into large spools (Fig. 1a). Therefore, to define samples from the cutting spool, the position on the cutting wire measured as the wire length from the start of the spool to the cutting position on the wire was used. In this paper, 2-km cutting wires were studied. A total of 21 diamonds on this sample were studied.

Due to its sensitivity to carbon materials and high spatial resolution, micro-Raman spectrometry is particularly suited in analyzing the property and structure of the individual diamonds [16]. A Renishaw InVia micro-Raman confocal spectrometer was used. Laser excitation at 514 nm (power= 1.175 mW/cm^2) and 785 nm (power=2.467 mW/cm^2) was applied, with laser spot size of 0.83 and 1.3 μm in diameter, respectively. An objective of ×50 was used to collect data resulting in a numerical aperture (NA) of 0.75. Scans were conducted from 100 to 3200 cm^{-1}. The exposure time for every scan was 10 s. Every scan was integrated once. The grating used was 1800 and 1200 lines/mm for 514 and 785 nm laser sources, respectively.

Confocal measurements were conducted to obtain depth profile information of the diamonds. A vertical displacement was obtained by a servo-controlled stage. A step height of 2 μm was used. The depth of focus (D.O.F) of this system was calibrated to be 4.2 μm using the transverse optical (TO) peak of a (100) Si prime wafer.

3 Results

Figure 2a shows a confocal image of the diamond particle obtained from the cutting wire at 2 km length under the Raman microscope at a magnification of ×50. The particle is ~20 μm in diameter. For taking the spectra, the tip of the diamond is in focus, while the region below the tip is out of focus. Later, we will describe confocal Raman measurements, which profile the diamond along the vertical, *z* direction.

Figure 2b shows the Raman spectra obtained from point "1". The laser used is 514 nm unless otherwise stated. A clear diamond peak is shown, centered at 1332 cm^{-1}. This is related to the T_{2g} symmetric vibration of the sp^3 carbon bond [17]. The peak at 2060 cm^{-1} is ascribed to the N_2 photoluminescence (from air). Another broad peak at 2450 cm^{-1} is also noticeable and is attributed to the second-order Raman of diamond which is 250 times weaker than its primary, 1332 cm^{-1} peak [18].

The full-width half max (FWHM) of the diamond particle was found to be 7 cm^{-1}. Single crystal diamonds have been shown to have a FWHM of 3 cm^{-1}. Chemical-vapor-deposited diamond films are known to show larger FWHM (9 cm^{-1}) [19]. Increase in FWHM is speculated to occur due to internal strains or polycrystallinity in diamond.

Raman spectra measured from point "2," however, is completely different. Figure 2c shows the presence of two broad peaks. The primary peaks are centered at 1350 and 1597 cm^{-1}. These are assigned the classic D band [20] and G band [21] for graphitic carbon, respectively.

The D band is induced by defects in graphite, while the G band in graphitic materials is due to the E_{2g} Raman active mode for sp^2 carbon [22]. The D band can be influenced by the remnant diamond phase (located at 1332 cm^{-1}) physically present around the graphitic phase. Further, we note that the G band is blue shifted from 1580 to 1597 cm^{-1} and is attributed to the nanocrystalline graphite as will be discussed in the next section [23, 16]. Additional peaks noted are the G′ peak at 2700 cm^{-1} and the D + G combination mode near 2945 cm^{-1}, both of which are attributed to defects [24].

Interestingly from Fig. 2c, a Si TO peak at 521 cm^{-1} was also observed. We note that the presence of Si was not found on fresh, uncut diamond particles (not shown). This supports the hypothesis that the graphitic phase could be due to the cutting process and not inherently present in the uncut diamond particle. The Si tends to stick to the soft graphitic phase during the cutting process. No evidence of SiC formation was found.

Graphitic phases were observed in only 3 of the 21 diamonds studied. This points to the rarity of the graphitization event. We further note that Raman spectroscopy was also performed on a fresh DCW, which had not undergone any cutting and the graphitic phase was never observed in the sample size (10 in number) of diamonds studied.

In order to understand the extent of the graphitic phase in diamond, we conducted confocal Raman spectroscopy at point "2" of the diamond particle. This series of spectra obtained are shown in Fig. 3a. The spectra are separated by 2 μm in the vertical *z* direction. The start of the confocal measurement occurs at the tip surface of the diamond particle and results in the spectrum labeled as "1" in Fig. 3a. Subsequent spectra clearly show the presence of the D and G graphitic bands (labeled 2 and 3). Additionally for spectra "3," the diamond T_{2g} at 1332 cm^{-1} is observed emerging from the graphitic D band (broad and centered at 1350 cm^{-1}). We note that the Raman scattering intensity of diamond as compared to graphite is 50 times weaker. Thus, the appearance of a strong diamond peak with graphitic peaks indicates largely the presence of the diamond phase rather than graphite. Further, the D.O.F of the Raman microscope is 4.2 μm. This implies that the diamond and graphitic phases could coexist within this length scale. Probing deeper into the particle reduces the D and G bands, while the T_{2g} diamond peak increases in peak intensity. At 14 μm laser penetration, the G band of the graphitic phase completely disappears and only the T_{2g} peak from the diamond remains. Regardless of the origin of the graphitic

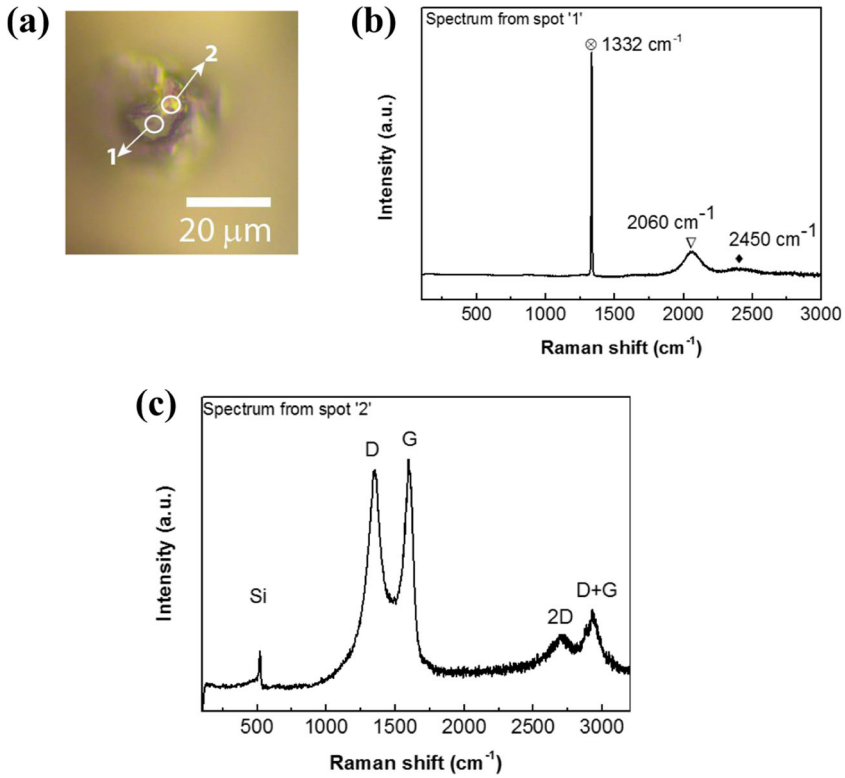

Fig. 2 **a** Image of diamond focused on the tip of the particle through the confocal microscope **b** Raman spectrum taken from *spot '1'*. *Encircled x* = diamond T_{2g} peak and *inverted triangle* = N_2 photoluminescence peak, *black diamond suit* = second-order peak for diamond **c** Raman spectrum taken from *spot '2'* showing the graphitic nature of the localized region

phase, the sequence of Raman spectra captures with high fidelity the graphitic phase within the diamond particle during Si wafering process.

Since the confocal measurement takes images of the diamond particle (as shown in Fig. 2a) for every z height, it is possible to reconstruct the shape of the diamond by stacking the individual images of the focused regions together in a 3D contour map. The result of such 3D reconstruction is shown in Fig. 3b for a stack of 74 images (z height difference of 0.2 μm). The arrow in the image shows the region where the graphitic phase was detected. Thus, a complete chemical and physical picture of the graphitic phase is obtained with our analysis.

While the diamond particle reported in Figs. 2 and 3 shows the existence of the graphitic phase, more often than not, the particles retained their diamond phase while only subtly changing Raman features. These minute shifts can be a source of valuable information providing insights to the diamond cutting process of Si. This is highlighted in the following example.

In Fig. 4a, two diamonds are noted in the micrograph. The arrow on top of the image indicates the drawing direction of the spool as the DCW performed the cutting. Line spectra were obtained across both the diamonds, starting from X= 42,938 μm to X=42,991 μm. The diamond T_{2g} peak is plotted in its peak intensity (left axis) and its peak position (right axis) in Fig. 4b. The peak intensity simply shows the presence of the diamond phase. However, the peak position shifts indicate the presence of built-in stresses [25]. It was confirmed separately (not shown) that fresh wires not subjected to cutting always showed the T_{2g} peak centered at 1332 cm^{-1}. Thus, any shift in the T_{2g} peak would be a result of the cutting process.

The T_{2g} peak shifts on the left diamond by 3.6 cm^{-1}. For the right diamond, the peak shifts by 2.0 cm^{-1}. Most remarkably, these shifts occur on the left side of both diamonds only and along the drawing direction of the wire. Clearly, the peaks are related to the cutting process and show the highly directional nature of the cut as the diamond particle presses against the Si ingot. From the peak shifts, it is possible to estimate the stresses in the diamond as will be shown in the discussion section.

4 Discussion

4.1 Nature of the graphitic phase in diamond particles

We propose that the graphitic phase observed in diamond particles is nanocrystalline in nature. Several pieces of evidence support this claim. First, evidence of formation of the nanocrystalline graphite is obtained by observing the full width at half maximum (FWHM) of the D band. It is noted that FWHM of the D band for amorphous carbon materials is between 200 and 300 cm^{-1} [26, 27]. On the other hand, single crystal graphite has an FWHM of 15 cm^{-1} [28]. In our

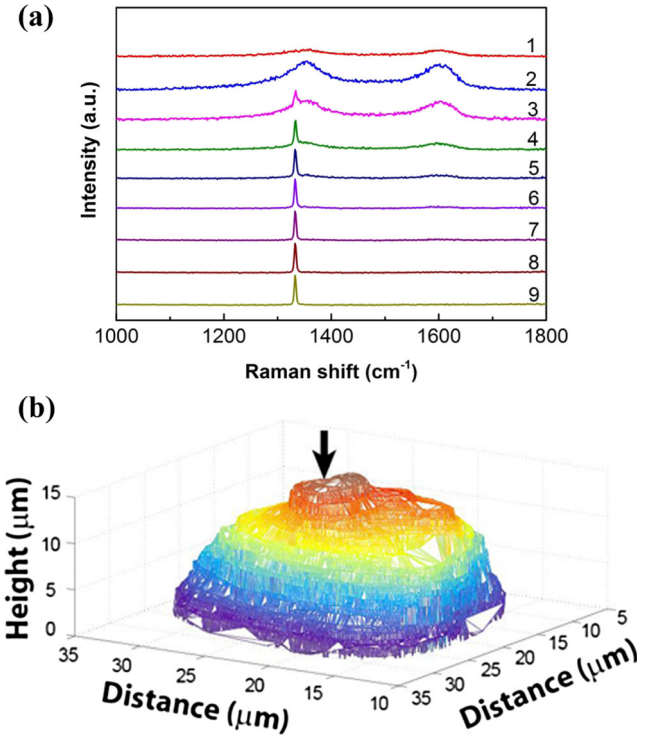

Fig. 3 **a** Confocal Raman spectroscopy of the graphitic region. *Red curve* (1) is sample surface. With increasing the number from 1 to 9 of the curve, the laser spot moves from the surface to the inner part of the sample with a step distance of 2 μm. **b** 3D reconstruction of the diamond particle as obtained from the confocal data using the focused region as a single slice at a specific *z* height. The *black arrow* shows where the graphitic region exists

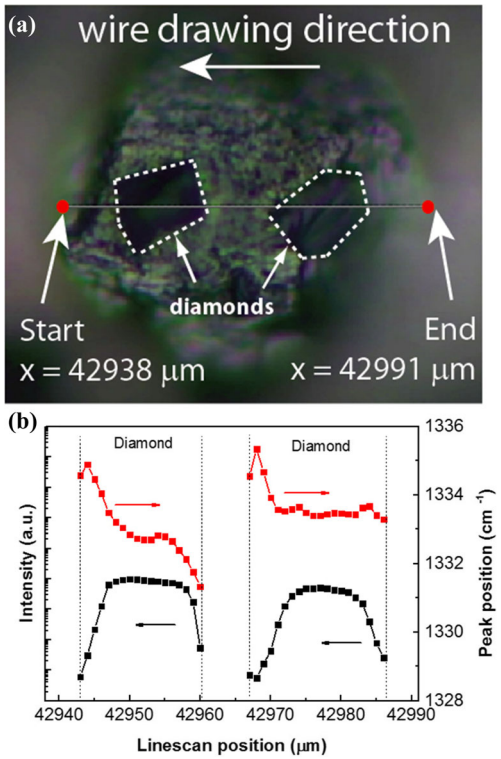

Fig. 4 **a** Micrograph of two diamond particles, which were subjected to Raman line can measurements. The *arrow* points toward the movement of the wire as it slid through the cutting groove. The start and end points show the beginning and ending of the Raman line scan. **b** Intensity (*left axis* in log scale for clarity and *black*) and peak position (*right axis* and *red*) as a function of laser position during the line scan. Both diamonds show a shift of the peak position on their left faces—a sign of compressive stresses

experimental results (Fig. 2c), the FWHM of the D band is 107.4 cm^{-1}, which is in between the FWHM of amorphous and single crystalline states.

Second, the dispersion of the D and G bands is studied as a function of two laser wavelengths—514 and 785 nm. This information is provided in Table 1. The peak positions are obtained by fitting two Lorentzian peak fitting functions to the D and G bands. As stated previously, the 514 nm laser results in the D and G bands to be positioned 1350 and 1597 cm^{-1}, respectively. For the 785 nm laser, the D and G bands are observed to be at 1314 and 1597 cm^{-1}, respectively.

Thus, the D band red shifts by 36 cm^{-1}. The behavior of D band red shifting is in accordance with the observation by several researchers, who predict dispersion behavior in nanocrystalline graphite of the D band at the rate of 40 to 50 cm^{-1}/eV [21, 16, 29, 30]. In our case, the energy difference between the two lasers (514 and 785 nm) is 0.83 eV. Accordingly, one should expect a D band downshift of 33 to 41 cm^{-1}. This is in excellent agreement with the experimental observation of 36 cm^{-1}.

No dispersion is observed for the G band. From the experimental results of Ferrari et al. [31], the G band position does not change with different laser wavelengths in crystalline graphite. However, the G band shows dispersion in amorphous carbon, and the dispersion increases with increasing degree of disorder [31, 32]. Based on these pieces of evidence, we conclude that diamond on the cutting wire transforms into nanocrystalline graphite instead of amorphous carbon material.

4.2 Size of nanocrystalline graphite

Knowing the intensities of the D and G bands allows us to calculate the size of the nanocrystalline graphite. The relationship between crystallite size and ratio of the integrated area between of I_d to I_g is given as [33]

Table 1 I_d and I_g peak positions obtained from spot "2" and its dependence on laser excitation wavelength

Laser wavelength (nm)	I_d peak position (cm^{-1})	I_g peak position (cm^{-1})
514	1350	1597
785	1314	1597

Spot "2" is in Fig. 2a

$$L_a = 2.4 \times 10^{-10} \lambda^4 \left(\frac{I_d}{I_g}\right)^{-1} \quad (1)$$

where L_a is the crystallite size (nm), λ is the laser wavelength used in nanometer (i.e., 514), and I_d and I_g are the integrated area under the D and G bands, respectively. The estimated nanocrystallite size of the graphite on the diamond particle as a function of depth is shown in Fig. 5. The crystallite size varies from 10 nm near the surface to 52 nm near the interface of graphite and diamond. Thus, with increasing vertical distance inside the sample, the crystallite size appears to increase.

4.3 State of stress of the diamond particles

It has been shown previously that hydrostatic stresses alone cannot induce graphitization of diamond. In order for phase transformation to occur, a combination of hydrostatic and shear stresses must be present [34]. These stresses must manifest themselves in some form in the diamond that can be detected by Raman. Indeed, compressive stresses cause blue shifts, while tensile stresses lead to red shifts in the Raman spectra [25].

Data from Fig. 4b show that blue shifts/compressive stress is produced in the diamond during Si cutting. The wavenumber shift is 3.6 cm^{-1} for the left diamond and 2.0 cm^{-1} for the right diamond. We have used the empirical model proposed by Hemley et al. [35] for 4 μm diamond powders under non-hydrostatic conditions and obtained 2.9 and 1.7 GPa for the two diamonds, respectively. These stresses are concentrated on the left face of the diamond particles and along the direction of the wire drawing—as is to be expected.

Compared to the stresses required to induce phase transformation in diamond, it is clear that these stresses are quite low. For example, theoretical investigations show that under uniaxial stresses on diamonds, a pressure of at least 285 GPa is required for metallization [36]. During wear, shear stresses on diamonds have to reach 95 GPa for graphitization to occur [37]. Finally, it has been suggested that plasticity in diamond can be induced at pressures ~150 GPa [38]. These stresses are much higher than the one uncovered on the stressed diamond in Fig. 4b. For graphitization to occur in DCWs due to the cutting process, we propose that either (1) the particles have to undergo a series of cutting events in which the stresses accumulate over time or (2) the diamonds encounter a single cutting event where the pressure on the diamond increases catastrophically causing it to convert to nanocrystalline graphite. The fact that a systematic trend in graphitic nanocrystalline grain sizes is found on the surface of diamond implies that the former mechanism (i.e., multiple stress events) could be the likely scenario. With each cutting event, grain refinement (i.e., breaking of larger grains into smaller sizes) of the topmost graphite layer occurs and leaves the subsurface graphite untouched. Since graphite is extremely soft compared to diamond, the stresses during the cutting events continue to drive the conversion of diamond to graphite at the subsurface interface.

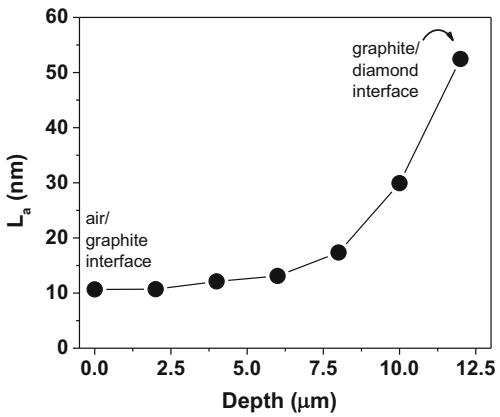

Fig. 5 The variation of graphitic nanocrystal size L_a as a function of depth inside the diamond particle shown in Fig. 3b. Here, depth=0 μm is the surface and depth >0 μm is inside the diamond particle

This conclusion is in line with the known mechanisms of diamond to graphite phase transformation proposed in literature. Zerda et al. [39] have suggested that the transformation occurs via either (1) direct "peeling" of the C atoms at the interface between (111) diamond and (002) oriented graphite or (2) groups of C atoms which detach from the interface and bond as sp^2 in tiny clusters. In case of mechanism "1," the G bands dominate the Raman signal for graphitization. Mechanism "2" leads to disoriented nanocrystallites of graphite and therefore to a larger D band signal.

Alternately, between these two extreme events, the particles while being subjected to cutting events can also be dislodged from their positions due to failure of the Ni film. Recall that the Ni film binds the diamonds to the stainless steel wire. Therefore, the compressive stresses obtained by our analysis provide a minimum estimate of the shear modulus of Ni films required to maintain embedded diamond particles on the Ni surface. Finally, the role of temperature during the cutting process needs to be addressed. Since a coolant is used during DCW sawing, large temperature increases (greater than tens of degrees) are not expected to occur [40].

5 Conclusions

Individual diamond particles 20 μm in diameter were obtained from a diamond-coated wire which had undergone PV-grade Si ingot cutting. Micro-Raman spectroscopy was conducted on these diamonds. Two conclusions can be drawn from our investigations. First, some of the diamonds showed the presence of nanocrystalline graphite coexisting with the diamond phase in the same particle. Using the model proposed by Cancado et al., we predict that the size of the nanocrystalline

graphitic phase varied from 10 nm near the surface to 52 nm at the graphite–diamond interface. On other diamonds, the presence of compressive stress could be detected. The stress was localized on regions which faced the Si ingot during the cutting process. Compressive stresses as high as 2.9 GPa were detected.

Based on these two observations, there appears to be a possibility that one of the reasons for the loss in efficiency during diamond-coated wire sawing could be the graphitization of the diamond particles. The graphitization can be a multi-step event where with each cutting, an increment in the local compressive stress state occurs. When the stress reaches a critical threshold, graphitization spontaneously occurs in a localized and confined volume within the diamond particle.

Acknowledgments Partial support under the US–India Partnership to Advance Clean Energy-Research (PACE-R) for the Solar Energy Research Institute for India and the United States (SERIIUS), funded jointly by the US Department of Energy (Office of Science, Office of Basic Energy Sciences, and Energy Efficiency and Renewable Energy), Solar Energy Technology Program, under Subcontract DE-AC36-08GO28308 to the National Renewable Energy Laboratory, Golden, Colorado, and the Government of India, through the Department of Science and Technology under Subcontract IUSSTF/JCERDC-SERIIUS/2012, is acknowledged. Raman equipment support by Professor Singamaneni's Soft Nanomaterials Lab is graciously acknowledged.

References

1. Bye J, Norheim L, Holme B, Nielsen O, Steinsvik S, Jensen S, Fragiacomo G, Lombardi I (2011) Industrialised diamond wire wafer slicing for high efficiency solar cells. In: Proceedings of the 26th European photovoltaic solar energy conference, WIP-Renewable Energies, Germany, pp 956–960
2. Gogotsi Y, Baek C, Kirscht F (1999) Raman microspectroscopy study of processing-induced phase transformations and residual stress in silicon. Semicond Sci Technol 14(10):936–944. doi:10.1088/0268-1242/14/10/310
3. Gogotsi Y, Zhou GH, Ku SS, Cetinkunt S (2001) Raman microspectroscopy analysis of pressure-induced metallization in scratching of silicon. Semicond Sci Technol 16(5):345–352. doi:10.1088/0268-1242/16/5/311
4. Hao W, Melkote SN (2012) Study of ductile-to-brittle transition in single grit diamond scribing of silicon: application to wire sawing of silicon wafers. J Eng Mater Technol 134(4):041011. doi:10.1115/1.4006177
5. Li XP, He T, Rahman M (2005) Tool wear characteristics and their effects on nanoscale ductile mode cutting of silicon wafer. Wear 259:1207–1214. doi:10.1016/j.wear.2005.12.020
6. Arefin S, Li XP, Cai MB, Rahman M, Liu K, Tay A (2007) The effect of the cutting edge radius on a machined surface in the nanoscale ductile mode cutting of silicon wafer. Proc Inst Mech Eng B J Eng Manuf 221(2):213–220. doi:10.1243/09544054jem568
7. Arefin S, Li XP, Rahman M, Liu K (2007) The upper bound of tool edge radius for nanoscale ductile mode cutting of silicon wafer. Int J Adv Manuf Technol 31(7–8):655–662. doi:10.1007/s00170-005-0245-0
8. Durazo-Cardenas I, Shore P, Luo X, Jacklin T, Impey SA, Cox A (2007) 3D characterisation of tool wear whilst diamond turning silicon. Wear 262(3–4):340–349. doi:10.1016/j.wear.2006.05.022
9. Jasinevicius RG, Duduch JG, Montanari L, Pizani PS (2012) Dependence of brittle-to-ductile transition on crystallographic direction in diamond turning of single-crystal silicon. Proc Inst Mech Eng B J Eng Manuf 226(B3):445–458. doi:10.1177/0954405411421108
10. Cai MB, Li XP, Rahman A (2007) Study of the temperature and stress in nanoscale ductile mode cutting of silicon using molecular dynamics simulation. J Mater Process Technol 192:607–612. doi:10.1016/j.jmatprotec.2007.04.028
11. Sopori B, Devayajanam S, Shet S, Guhabiswas D, Basnyat P, Moutinho H, Gedvilas L, Jones K, Binns J, Appel J (2013) Characterizing damage on Si wafer surfaces cut by slurry and diamond wire sawing. Paper presented at the 2013 I.E. 39th photovoltaic specialists conference. IEEE, New York. 10.1109/pvsc.2013.6744298
12. Holt A, Thogersen A, Rohr C, Bye J, Helgesen G, Nordseth O, Jensen SA, Norheim L, Nielsen O (2010) Surface structure of mono-crystalline silicon wafers produced by diamond wire sawing and by standard slurry sawing before and after etching in alkaline solutions. Paper presented at the 2010 35th IEEE photovoltaic specialists conference (PVSC). IEEE, New York. 10.1109/PVSC.2010.5614103
13. Hongchen M, Lang Z (2014) Mechanical behavior of diamond-sawn multi-crystalline silicon wafers and its improvement. Silicon 6(2):129–135. doi:10.1007/s12633-013-9170-2
14. Lewis IR, Edwards HGM (2001) Handbook of Raman spectroscopy: from the research laboratory to the process line. Practical spectroscopy, vol 28. Marcel Dekker, New York
15. Zhang Y, Tani Y, Murata J, Hashizume T (2014) Development of partially Ni-coated diamond abrasives for electroplated tools. Trans JSME 80:SMM0111. doi: 10.1299/transjsme.2014smm0111
16. Wang Y, Alsmeyer DC, Mccreery RL (1990) Raman-spectroscopy of carbon materials - structural basis of observed spectra. Chem Mater 2(5):557–563. doi:10.1021/Cm00011a018
17. Robertson J (2002) Diamond-like amorphous carbon. Mater Sci Eng R 37(4–6):129–281. doi:10.1016/S0927-796x(02)00005-0
18. Solin S, Ramdas A (1970) Raman spectrum of diamond. Phys Rev B 1(4):1687–1698. doi:10.1103/PhysRevB.1.1687
19. McCauley TS, Vohra YK (1994) Defect center in diamond thin films observed by micro-Raman and photoluminescence studies. Phys Rev B 49(7):5046–5049. doi:10.1103/Physrevb.49.5046
20. Tuinstra F, Koenig JL (1970) Raman spectrum of graphite. J Chem Phys 53(3):1126–1130. doi:10.1063/1.1674108
21. Matthews MJ, Pimenta MA, Dresselhaus G, Dresselhaus MS, Endo M (1999) Origin of dispersive effects of the Raman D band in carbon materials. Phys Rev B 59(10):R6585–R6588. doi:10.1103/Physrevb.59.R6585
22. Pimenta MA, Dresselhaus G, Dresselhaus MS, Cancado LG, Jorio A, Saito R (2007) Studying disorder in graphite-based systems by Raman spectroscopy. Phys Chem Chem Phys 9(11):1276–1291. doi:10.1039/B613962k
23. Cancado LG, Jorio A, Ferreira EHM, Stavale F, Achete CA, Capaz RB, Moutinho MVO, Lombardo A, Kulmala TS, Ferrari AC (2011) Quantifying defects in graphene via Raman spectroscopy at different excitation energies. Nano Lett 11(8):3190–3196. doi:10.1021/Nl201432g
24. Vidano RP, Fischbach DB, Willis LJ, Loehr TM (1981) Observation of Raman band shifting with excitation wavelength for carbons and graphites. Solid State Commun 39(2):341–344. doi:10.1016/0038-1098(81)90686-4
25. Sharma SK, Mao H, Bell P, Xu J (1985) Measurement of stress in diamond anvils with micro-Raman spectroscopy. J Raman Spectrosc 16(5):350–352. doi:10.1002/Jrs.1250160513

26. Huong PV (1991) Structural studies of diamond films and ultrahard materials by Raman and micro-Raman spectroscopies. Diam Relat Mater 1(1):33–41. doi:10.1016/0925-9635(91)90009-Y
27. Vohra YK, Mccauley TS (1994) Metastable phases of carbon during fracture of diamond under ultrahigh compressive stresses. Diam Relat Mater 3(8):1087–1090. doi:10.1016/0925-9635(94)90097-3
28. Hanfland M, Beister H, Syassen K (1989) Graphite under pressure: equation of state and first-order Raman modes. Phys Rev B 39(17): 12598–12603. doi:10.1103/PhysRevB.39.12598
29. Pocsik I, Hundhausen M, Koos M, Ley L (1998) Origin of the D peak in the Raman spectrum of microcrystalline graphite. J Non-Cryst Solids 227:1083–1086. doi:10.1016/S0022-3093(98)00349-4
30. Reich S, Thomsen C (2004) Raman spectroscopy of graphite. Philos T Roy Soc A 362:2271–2288. doi:10.1098/rsta.2004.1454
31. Ferrari AC, Robertson J (2001) Resonant Raman spectroscopy of disordered, amorphous, and diamond like carbon. Phys Rev B 64(7):075414. doi:10.1103/Physrevb.64.075414
32. Chu PK, Li LH (2006) Characterization of amorphous and nanocrystalline carbon films. Mater Chem Phys 96(2–3):253–277. doi:10.1016/J.Matchemphys.2005.07.048
33. Cancado LG, Takai K, Enoki T, Endo M, Kim YA, Mizusaki H, Jorio A, Coelho LN, Magalhaes-Paniago R, Pimenta MA (2006) General equation for the determination of the crystallite size L-a of nanographite by Raman spectroscopy. Appl Phys Lett 88(16): 163106. doi:10.1063/1.2196057
34. Gogotsi YG, Kailer A, Nickel KG (1998) Pressure-induced phase transformations in diamond. J Appl Phys 84(3):1299–1304. doi:10.1063/1.368198
35. Ji-an X, Ho-kwang M, Hemley RJ (2002) The gem anvil cell: high-pressure behaviour of diamond and related materials. J Phys Condens Matter 14(44):11549–11552. doi:10.1088/0953-8984/14/44/514
36. Van Camp P, Van Doren V, Devreese J (1992) Theoretical study of diamond under strong anisotropic stresses. Solid State Commun 84(7):731–733. doi:10.1016/0038-1098(92)90468-O
37. Chacham H, Kleinman L (2000) Instabilities in diamond under high shear stress. Phys Rev Lett 85(23):4904–4907. doi:10.1103/Physrevlett.85.4904
38. Mao H, Hemley R (1991) Optical transitions in diamond at ultra-high pressures. Nature 351(6329):721–724. doi:10.1038/351721a0
39. Pantea C, Qian J, Voronin GA, Zerda TW (2002) High pressure study of graphitization of diamond crystals. J Appl Phys 91(4): 1957–1962. doi:10.1063/1.1433181
40. Moller HJ (2004) Basic mechanisms and models of multi-wire sawing. Adv Eng Mater 6(7):501–513. doi:10.1002/adem.200400578